# Elucidating Substrate Promiscuity within the FabI Enzyme Family

Gabriel S. Freund,[†,‡,○] Terrence E. O'Brien,[†,§,○] Logan Vinson,[†] Dylan Alexander Carlin,[†,#]
Andrew Yao,[†] Wai Shun Mak,[†,§] Ilias Tagkopoulos,[†,∇] Marc T. Facciotti,[†,⊥] Dean J. Tantillo,[§]
and Justin B. Siegel[*,†,§,∥]

[†]Genome Center, University of California Davis, One Shields Avenue, Davis, California 95616, United States

[‡]Department of Mathematics, University of California Davis, Davis, California United States

[§]Department of Chemistry, University of California Davis, Davis, California United States

[∥]Department of Biochemistry & Molecular Medicine, University of CaliforniaDavis, Davis, California United States

[⊥]Department of Biomedical Engineering, University of California, Davis, California United States

[#]Biophysics Graduate Group, University of California Davis, Davis, California United States

[∇]Department of Computer Science, University of California Davis, Davis, California United States

Ⓢ *Supporting Information*

Experimentally Active

Compuational Prediction
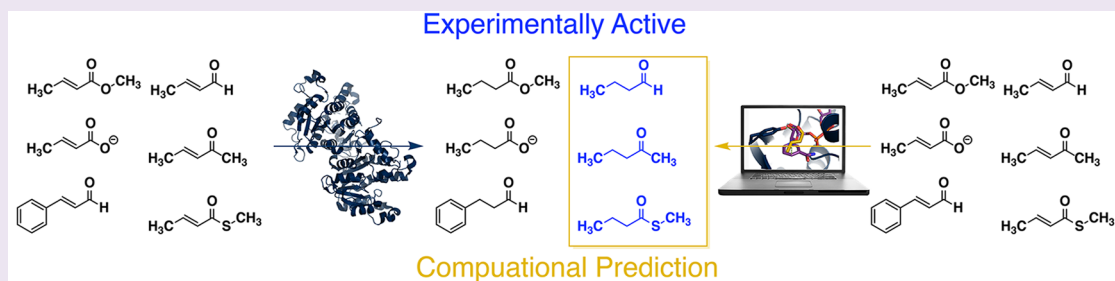
ABSTRACT: The rapidly growing appreciation of enzymes' catalytic and substrate promiscuity may lead to their expanded use in the fields of chemical synthesis and industrial biotechnology. Here, we explore the substrate promiscuity of enoyl-acyl carrier protein reductases (commonly known as FabI) and how that promiscuity is a function of inherent reactivity and the geometric demands of the enzyme's active site. We demonstrate that these enzymes catalyze the reduction of a wide range of substrates, particularly α,β-unsaturated aldehydes. In addition, we demonstrate that a combination of quantum mechanical hydride affinity calculations and molecular docking can be used to rapidly categorize compounds that FabI can use as substrates. The results here provide new insight into the determinants of catalysis for FabI and set the stage for the development of a new assay for drug discovery, organic synthesis, and novel biocatalysts.

Enzymes are promiscuous, catalyzing reactions beyond what they were specifically evolved for with widely varying rates.[1] The type of promiscuity observed is often categorized as either conditional, substrate, or catalytic. Conditional promiscuity occurs when catalysis is induced by altered reaction conditions (i.e., different pH or temperature). Substrate promiscuity is defined as the ability of an enzyme to catalyze the same chemical reaction for different substrates. Catalytic promiscuity is defined as the ability of an enzyme to catalyze chemically distinct reactions involving different types of transition states.[2] For example, tyrosine phosphatase has been shown to exhibit both catalytic and substrate promiscuity. Its ability to catalyze both phosphate and sugar hydrolysis reactions highlights the enzyme's catalytic promiscuity while its ability to utilize both mono and diester substrates demonstrates its substrate promiscuity.[3] In a biological context, some noncanonical promiscuous reactions have been postulated to be a critical factor in the evolution of new enzyme function.[4] The fields of biotechnology and synthetic chemistry

harness enzyme promiscuity to create and use enzymes with target substrates not found in nature.[2,5] In particular, the Old Yellow Enzyme family and other ene-reductases are used in industry for the reduction of numerous activated alkenes.[6]

In this study, we explore the substrate promiscuity of the enoyl-acyl carrier protein reductase family and we examine how the promiscuity is a function of both inherent reactivity of the substrate and geometric requirements of the enzyme. The canonical physiological function of enoyl-acyl carrier protein reductase (commonly referred to as FabI) is to reduce an enoyl acyl carrier protein (e.g., crotonyl-ACP) to its saturated form (Figure 1A).[7] This reaction is the rate limiting step in the type II fatty acid synthesis pathway. It is also well established that FabI exhibits substrate promiscuity on crotonyl Coenzyme A (CoA).[8] For both substrates, the proposed mechanism for the
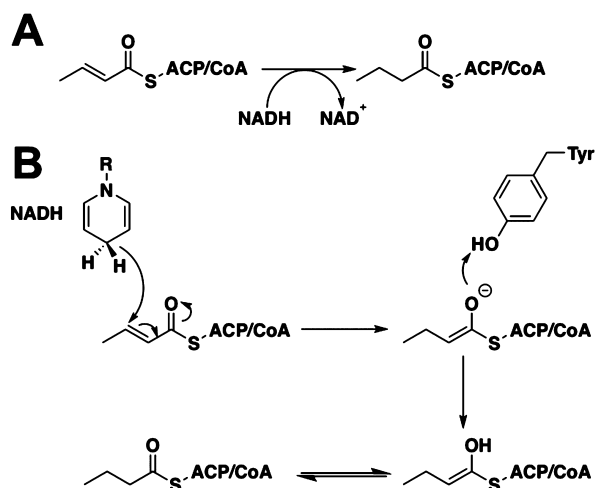
Figure 1. (A) The canonical reaction of FabI (EC 1.3.1.9), the reduction of crotonyl-ACP during the fourth and final step in type II fatty acid synthesis. It is also well established that FabI has promiscuous activity on crotonyl-CoA, a closely related substrate to crotonyl-ACP. (B) The proposed mechanism of FabI.

enzyme proceeds through a hydride transfer to the β-carbon, forming an enolate ion, which then accepts a proton from a

tyrosine residue. A keto−enol tautomerization forms the final product (Figure 1B).[9]

Here, we explored substrate promiscuity of FabI through a systematic investigation of five FabI orthologs against 13 substrates. The substrates vary in both geometry and in oxidation state. We evaluated if phylogenetic distance influenced enzyme behavior and therefore selected a set of five enzymes from two distinct parts of the phylogenetic tree whose sequence identities ranged from 19.2 to 73.5% (Figure 2 and Supporting Information Figure S1). We demonstrate promiscuous substrate activity on a wide range of substrates and demonstrate that this promiscuity is common across the five FabI's tested.

■ RESULTS AND DISCUSSION

Using the well-studied FabI from *P. falciparum* (pfFabI),[13,15] we conducted a sequence homology search using HMMER3[10] of the UniProt Representative Proteomes (rp75) for FabI homologues, which after filtering for redundancy and false positives through a CDHit,[11] resulted in a total of 2191 unique sequences being identified (Figure 2). We selected a subset of five FabI enzymes that covered four distinct kingdoms across the tree of life. In addition, we selected enzymes with sequence identities that range from 19 to 73.5% with an average value of 36.6% identity (Figure S1). Of the five enzymes selected, three had been previously characterized—from *E. coli* (ecFabI_<-
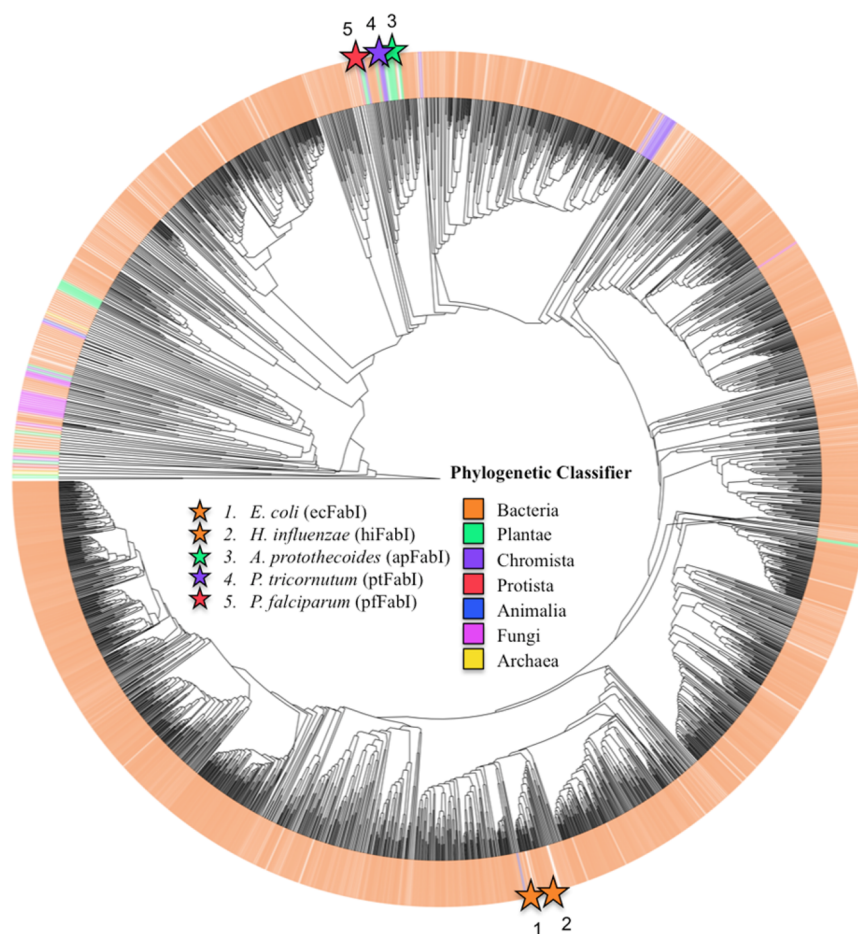
Figure 2. A phylogenetic tree of FabI proteins. Sequences were found through a HMMER search. Enzymes selected for functional characterization are highlighted with a star and kingdom meta information depicted by color. Selected enzymes are from a variety of clades and as evolutionarily distant as possible.
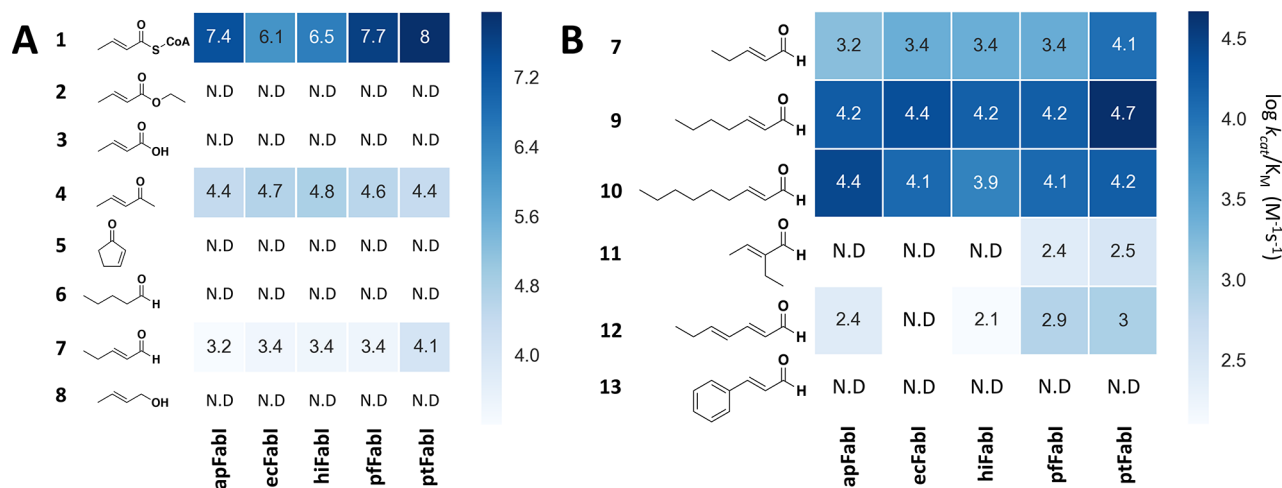
Figure 3. Heatmaps depicting the substrate promiscuity measured by observed apparent catalytic efficiency (k_{cat}/K_M in M^{-1} s^{-1}) on a logarithmic scale as determined by steady-state kinetics. Substrates in (A) differ by oxidation state, while those in (B) are α,β-unsaturated aldehydes which vary in chain length, branching position, and the addition of a phenyl ring. All calculated errors were below 15%. Substrate versus velocity curves and a full table of kinetic constants with standard errors can be found in Supporting Information Figure S2 and Table S3, respectively. The limit of detection for the assay conducted here is defined as 100 M^{-1} s^{-1} based on the observed rates being at least 2-fold higher than the background NADH oxidation rate at the highest substrate concentration. No observed activity is denoted as N.D (No Detection).

P0AEK4>), from *H. influenzae* (hiFabI_<P44432>), and from *P. falciparum* (pfFabI_<Q9BJJ9>). These three had previously been confirmed to have canonical FabI activity and express as soluble, active proteins in *E. coli*.[7,12,13] In addition, crystal structures have been reported for ecFabI[14] and pfFabI.[15] The other two enzymes selected were previously uncharacterized enzymes from a diatom, *P. tricornutum* (ptFabI_<B7FS72>), and from a green alga, *A. protothecoides* (apFabI_<A0A087SQF9>).

To explore the substrate promiscuity of FabI, we assessed the ability of the enzyme to catalyze the NADH mediated reduction of a range of structurally related substrates with varying degrees of oxidation states. The substrates selected were *trans*-crotonyl-coenzyme A (**1**; α,β-unsaturated thioester), ethyl *trans*-2-butenoate (**2**; α,β-unsaturated ester), *trans*-2-butenoic acid (**3**; α,β-unsaturated acid), 3-pentene-2-one (**4**), cyclopentenone (**5**; both α,β-unsaturated ketones), pentanal (**6**; saturated aldehyde), *trans*-2-pentenal (**7**; α,β-unsaturated aldehyde), and 2-buten-1-ol (**8**; α,β-unsaturated alcohol), all of which are pictured in Figures 3A. These panels of substrates were selected (A) for their similarity to the native substrate in that they contain α,β-unsaturated carbonyls (*i.e.*, α,β-unsaturated esters, acids, ketones and aldehydes) or (B) to test the potential for catalytic promiscuity (*i.e.*, the potential reduction of the carbonyl in a saturated aldehyde or the reduction of an olefin without being conjugated to a carbonyl). No detectible activity was observed in our assay with the majority of these substrates. However, all five FabI orthologs were found to reduce *trans*-2-pentenal as well as 3-pentene-2-one (Figure 3, Supporting Information Figures S2 and S3). Formation of the saturated aldehyde product was further validated using gas chromatography—mass spectrometry (Supporting Information Figure S4).
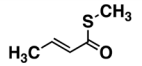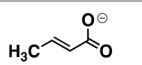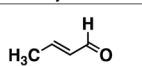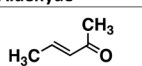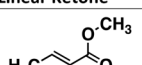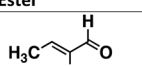
The catalytic efficiencies for each of the five FabI orthologs on *trans*-2-pentenal were 3−4 orders of magnitude lower than that of the native crotonyl-CoA substrate. While differences of 2 orders of magnitude in efficiency exist between the five FabI orthologs when utilizing the substrate crotonyl-CoA, less than an order of magnitude difference separates them when utilizing

trans-2-pentenal as a substrate. Similarly, the variance in catalytic efficiency when utilizing 3-pentene-2-one is within 1 order of magnitude. The efficiency of the five FabI orthologs on 3-pentene-2-one is over 1 order of magnitude higher than on *trans*-2-pentenal, except for ptFabI, where there is very little difference in efficiency between the aldehyde and ketone.

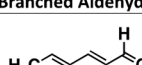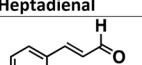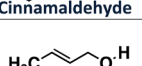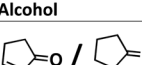Upon discovering that the entire family of FabI enzymes tested has substrate promiscuity for α,β-unsaturated aldehydes, we expanded our pool of α,β-unsaturated aldehyde substrates. The FabI enzymes were assessed for activity against a range of aldehydes that varied in both degree of branching, chain length, and conjugation (compounds **9**−**13** in Figure 3B). The production of the corresponding saturated aldehyde as a product was verified again using gas chromatography—mass spectrometry for *trans*-2-pentenal, *trans*-2-heptenal, and *trans*-2-nonenal (Supporting Information Figure S4).

trans-2-Pentenal (**7**), *trans*-2-heptenal (**9**), and *trans*-2-nonenal (**10**) exhibit roughly the same levels of catalytic efficiency across the five enzymes. Substrate branching leads to severely compromised activity; catalytic efficiency for (2E)-2-ethyl-2-butenal (**11**) decreased by roughly an order of magnitude for pfFabI and ptFabI relative to that for *trans*-2-pentenal. If a reaction was occurring for the branched substrate in apFabI, ecFabI, and hiFabI, it fell below our limit of detection. In addition, two degrees of unsaturation in the hydrocarbon chain (e.g., *trans,trans*-2,4-heptadienal (**12**)) led to decreased activity for all five enzymes by 1−2 orders of magnitude relative to that for *trans*-2-pentenal, with activity for ecFabI being below our limit of detection. Finally, the introduction of a phenyl ring (e.g., cinnamaldehyde (**13**)) led to a complete loss of activity among all enzymes tested.

Given the reactivity observed for different substrates, we hypothesized that both substrate shape and inherent reactivity are critical for catalysis. An ongoing question in our lab is to what degree does an enzyme take advantage of a substrate's inherent reactivity, *i.e.*, some substrates will have a higher tendency to be reduced than others, and does the enzyme take advantage of this preference? To evaluate the plausibility of these hypotheses, we conducted both quantum mechanical

Substrate	Log of Activity (log kcat/km)	S-Trans Substrate		S-Cis Substrate	
		Relative Hydride Affinity (kcal/mol)	Hydrogen Bond Score (Rosetta energy units)	Relative Hydride Affinity (kcal/mol)	Hydrogen Bond Score (Rosetta energy units)
COA Analog	7.1*	0.00	0.00	0.00	-0.52
Carboxylate	0.0	21.11	0.00	23.92	-0.70
Aldehyde	3.5	-5.02	0.00	-5.43	-0.66
Linear Ketone	4.6	-0.89	0.00	-0.16	-0.74
Ester	0.0	3.77	0.00	6.07	-0.57
Branched Aldehyde	2.5	-2.30	0.00	-2.90	-0.30
Heptadienal	2.6	0.33	0.00	0.60	-0.44
Cinnamaldehyde	0.0	-4.29	0.00	-4.15	0.00
Alcohol	0.0	34.02	0.00	36.84	-1.23
Cyclopentenone	0.0/ >2.0**	0.87	0.00	-4.70	-0.60

Figure 4. Results from QM and docking calculations on the substrates assayed in FabI, for both potential orientations of those substrates. Hydride affinities (free energies in kcal/mol) predicted with quantum mechanics (see Methods section) are relative to the predicted hydride affinity of the CoA analog. The hydrogen bond score (hb_sc of the ligand in Rosetta) of the ligand was identified as a potential metric for discriminating active substrates from the Rosetta docking simulations. Cells filled in green represent results where the calculations predicted activity and the enzyme was experimentally active. Cells filled in gray are where the calculations predict inactivity and no activity detected experimentally. Cells in red represent calculations that do not predict the experimental outcome correctly. *The rate listed here is for the full cofactor, not the truncated substrate examined in the QM and docking experiments. **The active 2-methylene-cyclopentenone (right) was not measured in our assay as the substrate is not commercially available but is reported as active by Liu et al.[29] The activity is denoted as greater than the lowest activity detected in our assay. The two cyclic ketones represent structures that are locked into either an s-cis or s-trans conformation.

(QM) calculations on the hydride-accepting ability of substrates in the absence of any protein, as a measure of the substrate's inherent reactivity, and molecular docking studies to examine substrate-enzyme shape complementarity. Both potential conformers, s-cis or s-trans, were evaluated, as which of these is the catalytically relevant conformation of the substrate is currently unknown (Figure 4, header). The hydride affinity for each substrate was calculated with Gaussian 09[18] at the SMD(water)[19]-B3LYP[20−24]/6-31+G(d,p) level of theory (Figure 4, relative hydride affinity). Hydride affinities for both conformers were similar, with a slight favoring of the s-cis conformation. Overall, our results imply that if a substrate's hydride affinity is 1 kcal/mol or lower, then it is predicted to be an active substrate. However, the notable exception to this rule

of thumb is cinnamaldehyde, which, despite having a negative relative hydride affinity score, had no detectable activity in our assay.

Besides the inherent reactivity toward hydride addition, whether or not a substrate fits appropriately into an active site is also undoubtedly important. For example, in FabI, there is a tyrosine side chain positioned to donate a proton to the enolate formed upon hydride addition (Figure 1B). Substrates that cannot position their carbonyl to interact favorably with this oxy-anion hole are less likely to undergo catalysis.[9] To determine the feasibility of binding in a productive orientation, each substrate (in both s-cis and s-trans conformations) was docked into FabI (PDB accession code 1NNU) using the Rosetta Modeling Suite[25−28] (Figure 4, hydrogen bond score)
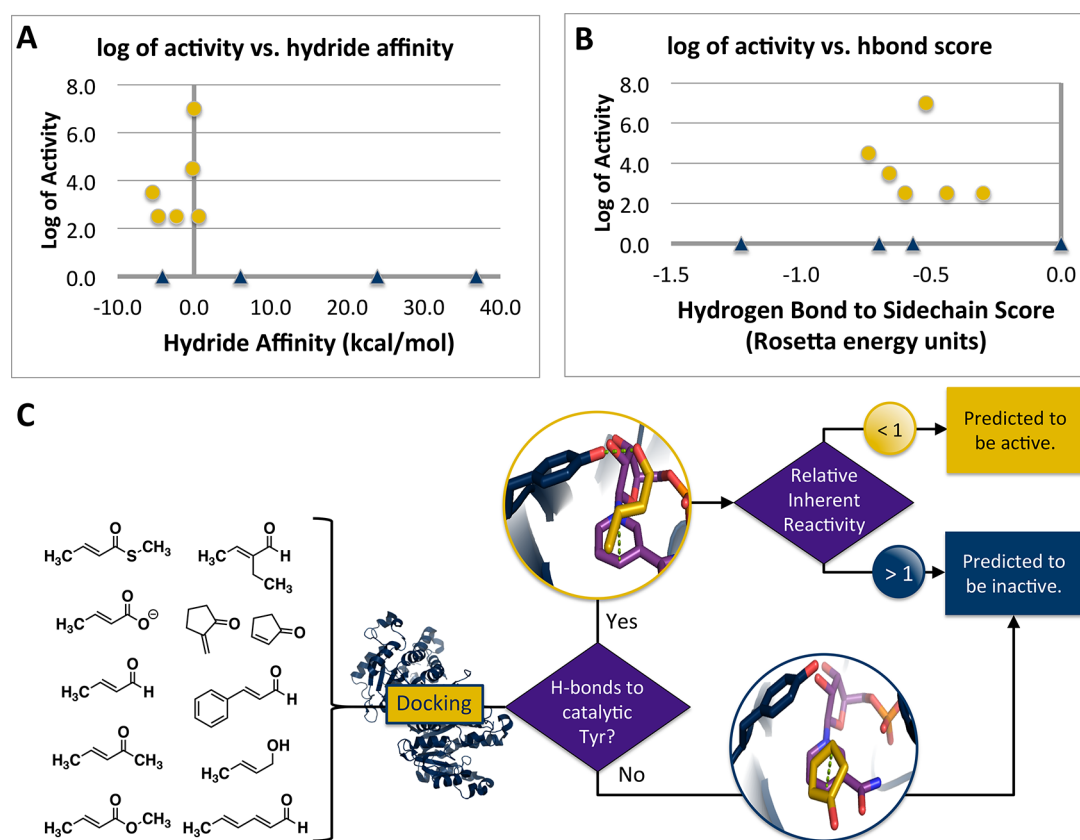
Figure 5. Evaluation of activity as a function of hydride affinity (A) or hydrogen bonding score in the predicted binding mode (B). Yellow circles correspond to substrates that had activity in our assay; blue triangles correspond to substrates that did not have activity. Neither metric alone is found to be accurate for prediction of function. (C) Decision tree for predicting potential new substrates for FabI based on a combination of the two metrics.

with a single constraint from the β-carbon of the substrate to the carbon of the cofactor from which the hydride is donated (see Supporting Information Figure S5).

From the docking calculation, neither the constraint nor the ligand interface energy (docking score) discriminated between active and inactive substrates for FabI (see Supporting Information Figures S5 and S6), but the ability to hydrogen bond to the catalytic tyrosine (TYR277 in 1NNU) appeared to have predictive value. The hydrogen bond scores for the s-cis conformers indicate that a variety of substrates can fit into the pocket in catalytically relevant orientations, including many substrates that did not have activity in the assay. Cinnamalde-hyde, which was expected to have FabI function based on its hydride affinity, had a hydrogen bond energy of zero in the docking calculations due to the presence of a bulky phenyl group, which distorts the pocket and forces the catalytic tyrosine away from its position in the crystal structure (see Supporting Information Figure S7). None of the s-trans substrates were able to find a pose in which they could hydrogen bond to Y277. This result implies that the catalytically relevant conformation is likely the s-cis conforma-tion.

Graphing the log of activity versus the relative inherent reactivity (Figure 5A) or versus the hydrogen bond score (Figure 5B) does not lead to a correlation that could be used to correctly predict the activity of all the substrates examined on their own. Attempts to find a formula combining both inherent reactivity and hydrogen bond score led to a qualitatively predictive but arbitrary model (see Supporting Information

Figure S17). Consequently, we suggest the use of the decision tree shown in Figure 5C to predict potential alternate substrates for FabI. On the basis of the tree, we predict that (E)-1-nitroprop-1-ene would be active while (E)-but-2-enenitrile would not be (see Supporting Information Figure S18); while both have appropriate inherent reactivity, the latter's geometry prevents productive binding. We look forward to the testing of this prediction.

The substrate promiscuity described here has implications for facilitating drug discovery efforts, as FabI is a drug target for tuberculosis,[30] microbial infections,[31] and malaria.[13,32] Current drug discovery approaches for FabI rely on the use of the expensive substrate crotonyl-CoA. The discovery of FabI activity with a less expensive substrate (e.g., trans-2-pentenal) has the potential to enable the development of more cost-effective high throughput assays. To illustrate this potential utility, we have demonstrated that inhibition of pfFabI by triclosan, a well-established FabI inhibitor, using trans-2-pentenal as a substrate, can be detected and quantified through the use of α,β-unsaturated aldehydes as substrates (Supporting Information Figure S11).

In this study, we have demonstrated that FabI has substrate promiscuity toward α,β-unsaturated aldehydes and has a high degree of substrate promiscuity for this reaction. In addition, we confirmed that FabI reduces linear α,β-unsaturated ketones.[29] We also demonstrated that a combination of molecular docking and quantum mechanics calculations on inherent reactivity can be used to predict substrate promiscuity of FabI. Finally, we demonstrate that this promiscuity for α,β-

unsaturated aldehydes disclosed here has the potential to decrease costs associated with drug discovery efforts that target FabI. Beyond drug discovery, enzyme promiscuity is a critical property often exploited for chemical synthesis[33] and enzyme engineering.[34−36] Studies such as this provide a critical starting point for chemists looking for a desired function beyond an enzyme's named reaction and will broaden the utility of FabI in the chemical sciences.

■ METHODS

Sequence Mining and Phylogenetic Analysis. Sequences were obtained using the amino acid sequence of pfFabI as a reference to find homologous sequences in the Representative Proteome 75 (rp75) database, yielding 6028 sequences. Redundant sequences were removed using a 90% sequence identity cutoff with the CD-HIT suite.[11] Sequences not in the interval of 250−350 residues were removed, and sequences not having the characteristic tyrosine-X_6-lysine catalytic motif were removed,[37] which resulted in 2191 sequences. The sequences were then aligned using a MUSCLE alignment in Geneious. Taxonomic information for each sequence was obtained using the UniprotKB. A phylogenetic tree was then constructed in Geneious using the UPGMA algorithm and a Jukes-Cantor genetic distance model. The tree image was then created using the GraPhlAn software tool.[16,17]

Substrate and Enzyme Selection. A protein and chemical space of 100 substrates and 2191 enzymes was considered, equating to roughly 10^5 possible enzyme−substrate combinations. To narrow this down to a tractable experimental space, we identified 65 unique combinations to provide a broad understanding of general specificity trends in the FabI family.

Substrates were selected for screening in the assay based on two key parameters: (1) geometry and (2) oxidation state. We were interested in the effects of different changes of the geometry, so substrates were chosen that had increased branching (**11**), increased conjugation (**12**), larger steric demand and increased conjugations (**13**), and increasing chain length (**7**, **9**, and **10**). It is known that FabI has activity on crotonyl-CoA, for which the oxidation state of the carbon in the thioester is +3. We selected a variety of other carbon centers that also had formal +3 oxidation states, such as an ester (**2**) and a carboxylic acid (**3**). The activity of this family of enzymes on α,β-unsaturated ketones has also been established,[18] for which the formal oxidation states of the carbonyl are +2. The use of an α,β-unsaturated ketone (**4**) served as a good benchmark for promiscuous activity, and the cyclic ketone (**5**) allowed for the probing of the active conformation. We also tested a variety of α,β-unsaturated aldehydes, which also have a formal oxidation state of +2 (see Supporting Information Figure S1 for additional information).

Enzymes were selected following three criteria: (1) Representation across multiple kingdoms from the tree of life, (2) a broad range of identity based on primary sequence, and (3) at least one for which there is a crystal structure with bound ligand. The first two metrics ensure that any observed functional trend observed is not unique within either a kingdom or to a specific FabI subfamily. The third metric ensured that there was a good starting point for molecular modeling in order to better understand the enzyme sequence-structure−function relationship.

Gene Synthesis and Plasmid Construction. Synthetic genes coding for FabI enzymes were codon optimized for *E. coli* expression and synthesized as linear dsDNA by IDT or Life Technologies. DNA and amino acid sequences can be found in Supporting Information Figures S12 and S13, respectively. The pET29b+ plasmid, containing a Kanamycin resistance gene and a C-terminal His-tag, was linearized with restriction enzymes *Eco*RI and NdeI sequentially and amplified using the Polymerase Chain Reaction (PCR) using the primers, FWD 5′-AATTCGAGCTCCGTCGACAAGCTTG-3′ and RVS 5′-ATGTATATCTCCTTCTTAAAGTTAA-3′. Genes were amplified by PCR using FWD 5′-TTAACTTTAAGAAGGAGATATACAT-3′ and RVS 5′-CAAGCTTGTCGACGGAGCTCGAATT-3′. The genes were assembled using Circular Polymerase Extension Cloning (CPEC)

as described by Quan and Tian[38] and transformed into electro-competent BLR(DE3) *E. coli* cells using a Micropulser Electroporator. Individual colonies were picked, grown overnight in Terrific Broth containing 50 μg/mL Kanamycin at 37 °C, and split for either mini-prepping and sequence verification *via* Sanger sequencing or for generation of glycerol stocks by mixing 1 mL of culture with 1 mL of 50% sterile glycerol. Glycerol stocks were frozen at −80 °C.

Expression and Purification. The cell pellet from a 25 mL overnight culture in Terrific Broth containing 50 μg/mL of Kanamycin at 37 °C was resuspended in 25 mL of autoinduction media (1 mM $MgSO_4$, 1% trace metals, 5% NPS (0.5 M $(NH_4)_2SO_4$, 1 M KH_2PO_4, 1 M Na_2HPO_4), 0.2% alpha-lactose, 0.05% glucose, 0.5% glycerol, 50 μg/mL Kanamycin in TB) and grown at 18 °C for 24 h for protein expression. Cells were centrifuged at 4700 rpm for 20 min, and supernatant was removed. Cells were either used immediately for protein purification or frozen at −20 °C. Cells were resuspended in 500 μL of wash buffer (50 mM HEPES at pH 7.5, 150 MM NaCl, 10 mM imidazole) and then combined with a lysis mix to achieve a final concentration of Bugbuster protein extraction reagent (Millipore) at 1×, 67 μg/mL PMSF, 0.53 mg mL^{-1} lysozyme, and 67 μg/mL DNase. Cells were placed on a rocker for 20 min at RT and then centrifuged at 14 700 rpm for 20 min. The supernatant was added to a gravity column containing 100 μL of HisPur cobalt resin (ThermoFisher), washed with six column volumes of wash buffer, and eluted with 250 μL of elution/protein buffer (50 mM HEPES at pH 7.5, 150 mM NaCl, 25 mM EDTA). Protein purity was assessed by SDS-PAGE (Supporting Information Figure S9), and concentrations were assessed *via* absorbance at 280 nm and the 260/280 ratio using an Epoch microplate spectrophotometer (Biotek). Extinction coefficients of proteins were calculated using the ExPASy ProtParam tool.[39]

Kinetic Assays. All kinetic assays were performed in 100 μL mixtures containing 500 μM NADH in 96 well plates. The K_M for NADH with no inhibitors was previously observed to be 20.5 μM for the FabI from *Candidatus* Liberibacter asiaticus.[41] In addition, a Brenda search of FabI (EC 1.3.1.9) shows that for wild type FabI, the reported K_M for NADH ranges from 3−85 μM. Therefore, we selected to conduct all assays in the presence of NADH, which we hypothesize will saturate the enzyme. Different substrate and enzyme concentrations were utilized for each enzyme−substrate combination. For *trans*-2-pentenal, *trans*-2-heptenal, 2-ethyl-2-butenal, *trans,trans*-2,4-heptadienal, ethyl *trans*-2-butenoate, cinnamaldeyde, 3-pentene-2-one, 2-cyclopentene-1-one, *trans*-2-butenoic acid, pentanal, and 2-butene-1-ol, 10 mM of each substrate was serially diluted 2-fold seven times. For *trans*-2-nonenal, 1 mM was serially diluted 2-fold seven times. For 3-pentene-2-one and 2-buten-1-ol, a stereochemically pure all *trans* substrate was not commercially available. Those substrates were assayed as a mixture of *cis* and *trans* isomers. For all assays, a negative control with no substrate was used. Between 2 and 12 μM enzyme was used for *trans*-2-pentenal; 1−4 μM for *trans*-2-heptenal and *trans*-2-nonenal; 9−33 μM for (2E)-2-ethyl-2-butenal; 18−75 μM for *trans,trans*-2,4-heptadienal; 11−71 μM for ethyl *trans*-2-butenoate; 10−47 μM for both cinnamalydehyde and cyclopentene-1-one; 3.2−20 μM for 3-pentene-2-one; and 22−35 μM for *trans*-2-butenoic, pentanal, and butene-1-ol. It should be noted that enzyme concentration was normalized in the calculation of the apparent kinetic constants.

Crotonyl-CoA required much more variable conditions for each enzyme. Data using 0.4 μM of ecFabI vs 2 mM crotonyl-CoA serially diluted 2-fold was combined with data using 43 nM ecFabI vs 2 mM crotonyl-CoA. Similarly, data using 0.4 μM hiFabI vs 2 mM crotonyl-CoA serially diluted 2-fold was combined with data using 39 nM hiFabI vs 2 mM serially diluted crotonyl-CoA. Then, 9 nM pfFabI was used vs 200 μM crotonyl-CoA serially diluted 2-fold. Next, 25 nM apFabI was used vs 2 mM crotonyl-CoA serially diluted 2-fold. Finally, 11 nM of ptFabI was used vs 125 μM crotonyl-CoA serially diluted 2-fold.

Due to the various hydrophobicities of the substrates, different conditions were employed to bring substrates into solution. For ethyl *trans*-2-butenoate, butenoic acid, 3-pentene-2-one, 2-cyclopentene-1-one, pentanal, 2-butene-1-ol, and cinnamaldehyde, 1.25% DMSO and

1.25% Triton X-100 final concentrations were used to bring these substrates into solution. For 2,4-heptadienal, 2.5% DMSO final concentration was used. A 1.25% DMSO final concentration was used for (2E)-2-ethyl-2-butenal. For *trans*-2-pentenal, *trans*-2-heptenal, and *trans*-2-nonenal, a 1.25% DMSO final concentration and a 0.025% Triton X-100 final concentration were used. No extra reagents were needed to bring Crotonyl-CoA into solution.

To test for the effects of solvents on catalytic efficiency, k_{cat}/K_M was measured for ptFabI on *trans*-2-pentenal under the following conditions: (1) 1.25% DMSO and 1.25% Triton X-100 final concentrations, (2) 1.25% DMSO, (3) 1.25% Triton X-100, (4) and no DMSO or Triton X-100. Catalytic efficiencies were all within 2 orders of magnitude of each other. Substrate versus velocity curves are presented in Supporting Information Figure S10.

Enzyme activity was monitored by the oxidation of NADH at 340 nm over the course of an hour using an Epoch microplate spectrophotometer. Due to the one-to-one stoichiometric ratio between NADH and the various substrates, the oxidation of 1 mol of NADH corresponds to the reduction of 1 mol of one of the substrates. Rates were measured in OD/min and converted to M/min using an NADH standard curve. From Supporting Information Figure 2, most plots were linear on non-crotonyl-CoA substrates, and therefore apparent k_{cat}/K_M was determined by taking the slope of the fitted line. However, ptFabI on *trans*-2-pentenal and *trans*-2-heptenal has Michaelis−Menten kinetics. The linear portions of the curves were used for apparent k_{cat}/K_M. On crotonyl-CoA, under our conditions, ecFabI, hiFabI, and pfFabI have linear rate vs substrate plots. ApFabI shows Michaelis−Menten kinetics, so the linear portion of this curve was used for apparent k_{cat}/K_M. PtFabI is observed to have substrate inhibition on crotonyl-CoA. The linear portion of the curve was used to calculate the apparent k_{cat}/K_M for ptFabI.

Gas Chromatography−Mass Spectrometry. The saturated aldehyde products for the substrates *trans*-2-pentenal, *trans*-2-heptenal, and *trans*-2-nonenal were validated using gas chromatography−mass spectrometry and compared to internal reference spectra for *trans*-2-pentenal and *trans*-2-nonenal, and *trans*-2-heptenal was compared to the NIST spectrum.[40] Gas chromatography−mass spectrometry parameters along with the spectra can be found in Supporting Information Figure S4.

Triclosan Inhibition Assay. Stock solutions of 1 mM, 5 μM, and 100 nM triclosan were prepared by dissolving triclosan into pure DMSO and then diluting 100 fold to yield 10 μM, 50 nM, and 1 nM triclosan in protein buffer (1% final DMSO). The kinetic assay described above was run with pfFabI and *trans*-2-pentenal, but with 10 μM, 50 nM, or 1 nM triclosan spiked in. In addition, secondary effluent from Woodland, CA wastewater was collected, sterile filtered, and buffered to pH 7.5, see Supporting Information Figure S11.

Quantum Mechanics Calculations. QM calculations were performed with Gaussian 09.[18] Minima were located using B3LYP[20−24]/6-31+G(d,p) with the SMD continuum solvation[19] method using water. Stationary points were confirmed as minima using harmonic vibrational analysis (no imaginary frequencies for minima). Structures used for calculations are provided in the Supporting Information, and computed energies are shown in Figure S8.

Docking Calculations. A single crystal structure of FabI (PDB ID: 1NNU) was minimized using a constrained FastRelax procedure from the Rosetta modeling suite.[25−28] The different substrates were then docked using the constraint described above (see Supporting Information Figures S5 and S6 for additional details on constraints). A total of 500 docking runs per substrate were performed to ensure that sampling was sufficient. The resulting structures were then filtered by (1) their ability to meet the constraints, structures that did not satisfy the constraints were not considered; (2) total protein energy, the lowest five structures in total protein energy were considered; and (3) the structure with the most negative hbond_sc score was selected from those five. An example docking simulation is provided in the Supporting Information.

ASSOCIATED CONTENT

Ⓢ Supporting Information

The Supporting Information is available free of charge on the ACS Publications website at DOI: 10.1021/acschem-bio.7b00400.

> Main Supplemental Information (PDF)
> S-cis geometries for substrates from QM calcs (ZIP)
> S14_aligned FabI sequences for the tree (TXT)
> S15_FabI taxonomy information (PDF)
> S16 Sample of the input files used in Rosetta calculations (ZIP)
> S-trans geometries for substrates from QM calcs (ZIP)

AUTHOR INFORMATION

Corresponding Author
*E-mail: jbsiegel@ucdavis.edu.

ORCID ⓘ
Terrence E. O'Brien: 0000-0002-5621-5065
Dean J. Tantillo: 0000-0002-2992-8844

Author Contributions
○Contributed equally to the manuscript

Notes
The authors declare no competing financial interest.

REFERENCES

(1) Khersonsky, O., and Tawfik, D. S. (2010) Enzyme promiscuity: a mechanistic and evolutionary perspective. *Annu. Rev. Biochem.* 79, 471−505.

(2) Hult, K., and Berglund, P. (2007) Enzyme promiscuity: mechanism and applications. *Trends Biotechnol.* 25, 231−238.

(3) Srinivasan, B., Marks, H. R., Mitra, S., Smalley, D. M., and Skolnick, J. (2016) Catalytic and substrate promiscuity: Distinct multiple chemistries catalyzed by phosphatase domain of receptor protein tyrosine phosphatase. *Biochem. J.* 473, 2165.

(4) Pandya, C., Farelli, J. D., Dunaway-Mariano, D., and Allen, K. N. (2014) Enzyme promiscuity: engine of evolutionary innovation. *J. Biol. Chem.* 289, 30229−30236.

(5) Kan, S. B. J., Lewis, R. D., Chen, K., and Arnold, F. H. (2016) Directed evolution of cytochrome c for carbon−silicon bond formation: Bringing silicon to life. *Science* 354, 1048−1051.

(6) Toogood, H. S., and Scrutton, N. S. (2014) New developments in 'ene'-reductase catalysed biological hydrogenations. *Curr. Opin. Chem. Biol.* 19, 107−115.

(7) Heath, R. J., and Rock, C. O. (1995) Enoyl-acyl carrier protein reductase (fabI) plays a determinant role in completing cycles of fatty acid elongation in Escherichia coli. *J. Biol. Chem. 270*, 26538–26542.

(8) Bergler, H., Wallner, P., Ebeling, A., Leitinger, B., Fuchsbichler, S., Aschauer, H., Kollenz, G., Hogenauer, G., and Turnowsky, F. (1994) Protein EnvM is the NADH-dependent enoyl-ACP reductase (FabI) of Escherichia coli. *J. Biol. Chem. 269*, 5493–5496.

(9) Rafferty, J. B., Simon, J. W., Baldock, C., Artymiuk, P. J., Baker, P. J., Stuitje, A. R., Slabas, A. R., and Rice, D. W. (1995) Common themes in redox chemistry emerge from the X-ray structure of oilseed rape (Brassica napus) enoyl acyl carrier protein reductase. *Structure 3*, 927–938.

(10) Finn, R. D., Clements, J., and Eddy, S. R. (2011) HMMER web server: interactive sequence similarity searching. *Nucleic Acids Res. 39*, W29–W37.

(11) Huang, Y., Niu, B., Gao, Y., Fu, L., and Li, W. (2010) CD-HIT Suite: a web server for clustering and comparing biological sequences. *Bioinformatics 26*, 680–682.

(12) Marcinkeviciene, J., Jiang, W., Kopcho, L. M., Locke, G., Luo, Y., and Copeland, R. A. (2001) Enoyl-ACP reductase (FabI) of Haemophilus influenzae: steady-state kinetic mechanism and inhibition by triclosan and hexachlorophene. *Arch. Biochem. Biophys. 390*, 101–108.

(13) Surolia, N., and Surolia, A. (2001) Triclosan offers protection against blood stages of malaria by inhibiting enoyl-ACP reductase of Plasmodium falciparum. *Nat. Med. 7*, 167–173.

(14) Rafi, S., Novichenok, P., Kolappan, S., Zhang, X., Stratton, C. F., Rawat, R., Kisker, C., Simmerling, C., and Tonge, P. J. (2006) Structure of acyl carrier protein bound to FabI, the FASII enoyl reductase from Escherichia coli. *J. Biol. Chem. 281*, 39285–39293.

(15) Perozzo, R., Kuo, M., Sidhu, A., Valiyaveettil, J. T., Bittman, R., Jacobs, W. R., Jr., Fidock, D. A., and Sacchettini, J. C. (2002) Structural elucidation of the specificity of the antibacterial agent triclosan for malarial enoyl acyl carrier protein reductase. *J. Biol. Chem. 277*, 13106–13114.

(16) Kearse, M., Moir, R., Wilson, A., Stones-Havas, S., Cheung, M., Sturrock, S., Buxton, S., Cooper, A., Markowitz, S., Duran, C., Thierer, T., Ashton, B., Meintjes, P., and Drummond, A. (2012) Geneious Basic: an integrated and extendable desktop software platform for the organization and analysis of sequence data. *Bioinformatics 28*, 1647–1649.

(17) Asnicar, F., Weingart, G., Tickle, T. L., Huttenhower, C., and Segata, N. (2015) Compact graphical representation of phylogenetic data and metadata with GraPhlAn. *PeerJ 3*, e1029.

(18) Frisch, M. J., Trucks, G. W., Schlegel, H. B., Scuseria, G. E., Robb, M. A., Cheeseman, J. R., Scalmani, G., Barone, V., Mennucci, B., Petersson, G. A., Nakatsuji, H., Caricato, M., Li, X., Hratchian, H. P., Izmaylov, A. F., Bloino, J., Zheng, G., Sonnenberg, J. L., Hada, M., Ehara, M., Toyota, K., Fukuda, R., Hasegawa, J., Ishida, M., Nakajima, T., Honda, Y., Kitao, O., Nakai, H., Vreven, T., Montgomery, J. A., Peralta, J. E., Ogliaro, F., Bearpark, M., Heyd, J. J., Brothers, E., Kudin, K. N., Staroverov, V. N., Kobayashi, R., Normand, J., Raghavachari, K., Rendell, A., Burant, J. C., Iyengar, S. S., Tomasi, J., Cossi, M., Rega, N., Millam, J. M., Klene, M., Knox, J. E., Cross, J. B., Bakken, V., Adamo, C., Jaramillo, J., Gomperts, R., Stratmann, R. E., Yazyev, O., Austin, A. J., Cammi, R., Pomelli, C., Ochterski, J. W., Martin, R. L., Morokuma, K., Zakrzewski, V. G., Voth, G. A., Salvador, P., Dannenberg, J. J., Dapprich, S., Daniels, A. D., Farkas, Foresman, J. B., Ortiz, J. V., Cioslowski, J., and Fox, D. J. (2009) *Gaussian 09*, revision B.01, Wallingford, CT.

(19) Marenich, A. V., Cramer, C. J., and Truhlar, D. G. (2009) Universal Solvation Model Based on Solute Electron Density and on a Continuum Model of the Solvent Defined by the Bulk Dielectric Constant and Atomic Surface Tensions. *J. Phys. Chem. B 113*, 6378–6396.

(20) Becke, A. D. (1993) A new mixing of Hartree−Fock and local density-functional theories. *J. Chem. Phys. 98*, 1372–1377.

(21) Becke, A. D. (1993) Density-functional thermochemistry. III. The role of exact exchange. *J. Chem. Phys. 98*, 5648–5652.

(22) Lee, C., Yang, W., and Parr, R. G. (1988) Development of the Colle-Salvetti correlation-energy formula into a functional of the electron density. *Phys. Rev. B: Condens. Matter Mater. Phys. 37*, 785–789.

(23) Tirado-Rives, J., and Jorgensen, W. L. (2008) Performance of B3LYP Density Functional Methods for a Large Set of Organic Molecules. *J. Chem. Theory Comput. 4*, 297–306.

(24) Stephens, P. J., Devlin, F. J., Chabalowski, C. F., and Frisch, M. J. (1994) Ab Initio Calculation of Vibrational Absorption and Circular Dichroism Spectra Using Density Functional Force Fields. *J. Phys. Chem. 98*, 11623–11627.

(25) Meiler, J., and Baker, D. (2006) ROSETTALIGAND: Protein–small molecule docking with full side-chain flexibility. *Proteins: Struct., Funct., Genet. 65*, 538–548.

(26) Fleishman, S. J., Leaver-Fay, A., Corn, J. E., Strauch, E.-M., Khare, S. D., Koga, N., Ashworth, J., Murphy, P., Richter, F., Lemmon, G., Meiler, J., and Baker, D. (2011) RosettaScripts: A Scripting Language Interface to the Rosetta Macromolecular Modeling Suite. *PLoS One 6*, e20161.

(27) Combs, S. A., DeLuca, S. L., DeLuca, S. H., Lemmon, G. H., Nannemann, D. P., Nguyen, E. D., Willis, J. R., Sheehan, J. H., and Meiler, J. (2013) Small-molecule ligand docking into comparative models with Rosetta. *Nat. Protoc. 8*, 1277–1298.

(28) Song, Y., DiMaio, F., Wang, R. Y.-R., Kim, D., Miles, C., Brunette, T. J., Thompson, J., and Baker, D. (2013) High-Resolution Comparative Modeling with RosettaCM. *Structure 21*, 1735–1742.

(29) Liu, J., Wu, J., and Li, Z. (2014) Enoyl acyl carrier protein reductase (FabI) catalyzed asymmetric reduction of the C[double bond, length as m-dash]C double bond of [small alpha],[small beta]-unsaturated ketones: preparation of (R)-2-alkyl-cyclopentanones. *Chem. Commun. 50*, 9729–9732.

(30) Lu, X. Y., You, Q. D., and Chen, Y. D. (2010) Recent progress in the identification and development of InhA direct inhibitors of Mycobacterium tuberculosis. *Mini-Rev. Med. Chem. 10*, 182–193.

(31) McMurry, L. M., Oethinger, M., and Levy, S. B. (1998) Triclosan targets lipid synthesis. *Nature 394*, 531–532.

(32) Thota, S., and Yerra, R. (2016) Drug Discovery and Development of Antimalarial Agents: Recent Advances. *Curr. Protein Pept. Sci. 17*, 275–279.

(33) Koeller, K. M., and Wong, C.-H. (2001) Enzymes for chemical synthesis. *Nature 409*, 232–240.

(34) Mak, W. S., Tran, S., Marcheschi, R., Bertolani, S., Thompson, J., Baker, D., Liao, J. C., and Siegel, J. B. (2015) Integrative genomic mining for enzyme function to enable engineering of a non-natural biosynthetic pathway. *Nat. Commun. 6*, 10005.

(35) Siegel, J. B., Smith, A. L., Poust, S., Wargacki, A. J., Bar-Even, A., Louw, C., Shen, B. W., Eiben, C. B., Tran, H. M., Noor, E., Gallaher, J. L., Bale, J., Yoshikuni, Y., Gelb, M. H., Keasling, J. D., Stoddard, B. L., Lidstrom, M. E., and Baker, D. (2015) Computational protein design enables a novel one-carbon assimilation pathway. *Proc. Natl. Acad. Sci. U. S. A. 112*, 3704–3709.

(36) Gordon, S. R., Stanley, E. J., Wolf, S., Toland, A., Wu, S. J., Hadidi, D., Mills, J. H., Baker, D., Pultz, I. S., and Siegel, J. B. (2012) Computational Design of an α-Gliadin Peptidase. *J. Am. Chem. Soc. 134*, 20513–20520.

(37) White, S. W., Zheng, J., Zhang, Y. M., and Rock (2005) The structural biology of type II fatty acid biosynthesis. *Annu. Rev. Biochem. 74*, 791–831.

(38) Quan, J., and Tian, J. (2009) Circular Polymerase Extension Cloning of Complex Gene Libraries and Pathways. *PLoS One 4*, e6441.

(39) Wilkins, M. R., Gasteiger, E., Bairoch, A., Sanchez, J. C., Williams, K. L., Appel, R. D., and Hochstrasser, D. F. (1999) Protein identification and analysis tools in the ExPASy server. *Methods Mol. Biol. 112*, 531–552.

(40) Mass Spectra, In *NIST Chemistry WebBook, NIST Standard Reference Database Number 69* (Mallard, E. P. J. L. a. W. G., Ed.), NIST Mass Spec Data Center, National Institute of Standards and Technology, Gaithersburg, MD.

(41) Jiang, L., Gao, Z., Li, Y., Wang, S., and Dong, Y. (2014) Crystal structures and kinetic properties of enoyl-acyl carrier protein reductase I from *Candidatus Liberibacter asiaticus*. *Protein Sci. 23*, 366−377.